

# Towards Routine 2-Step Based IMRT/IMAT Treatment Planning in the Clinic

Mark Gainey<sup>\*1</sup>, Kostyantyn Holubyev<sup>2</sup>, Klaus Bratengeier<sup>3</sup>

<sup>\*1</sup>Department of Radiation Oncology, University Medical Centre Freiburg, Robert Koch Strasse 3, 79106 Freiburg, Germany

<sup>2,3</sup>Department of Radiation Oncology, University Hospital Wuerzburg, Josef Schneider Strasse 11, 97080 Wuerzburg, Germany

<sup>\*1</sup>mark.gainey@uniklinik-freiburg.de; <sup>2</sup>holubyev\_k@klinik.uni-wuerzburg.de; <sup>3</sup>bratengeier\_k@klinik.uni-wuerzburg.de

**Abstract-** The purpose of this work is to describe the automation of 2-Step IMRT/IMAT segmentation. 2-Step IMRT/IMAT employs analysis of the PTV-OAR topology to determine the initial segment shapes for each gantry angle. Previous retrospective planning studies by the authors have shown that the quality of 2-Step IMRT/IMAT plans is at least as good as that of plans calculated based solely upon the optimization module in commercial treatment planning system (TPS) software. Hitherto the generation of the 2-Step segment shapes was performed manually employing the TPS, a time consuming process requiring approximately 5 minutes per PTV-OAR pair for each gantry angle. The software was written in C++ programming language and tested to process the structure set files to generate the 2-Step segments. Six clinical prostate cases incorporating a simultaneously integrated boost were employed to test segment generation for a typical seven field IMRT using the Synergy linac and BeamModulator MLC commissioned in the Pinnacle TPS available at the University Hospital Wuerzburg. Additionally, two clinical paraspinal tumour cases were also used to test segment generation for IMAT. The C++ classes were designed to be extensible for other MLCs and TPSs, which permit seeding of the optimiser with segment forms. For each PTV-OAR pair, a conformal (zeroth order), OAR blocked (first order) and “dose saturation” (second order) segment was automatically generated employing the BEV projection of the PTV and OAR. Subsequently these segment shapes were sequenced into deliverable MLC segments and exported to the TPS as IMRT or VMAT plans. For the prostate cases the mean time per generated segment was  $36 \pm 6$  ms (total 70 segments). For the paraspinal tumour cases, three complete arcs were generated with  $2^\circ$  spacing per control point (179 segments for a complete rotation). The total time taken was 13.1 and 12.0 s (537 segments) or 24 ms and 22 ms per segment respectively. These exported plans may be further optimized by the TPS. Alternatively the software may be used as the basis for adaption of treatment plans on the basis of daily cone beam CT (CBCT) studies. This work demonstrates the automatic generation of 2-Step IMRT and IMAT cases for the Pinnacle TPS. It enables more comprehensive planning studies to be performed.

**Keywords-** Radiotherapy; Treatment Planning; IMRT; VMAT; Adaption

## I. INTRODUCTION

Volumetric modulated arc therapy (VMAT) [1], is a variant of intensity modulated arc therapy (IMAT) [2], but unlike the latter includes the relevant machine parameters in the optimization process. Recently, many articles have been published regarding the merits of VMAT over intensity modulated radiotherapy (IMRT), and strategies for optimizing VMAT treatment planning [3-7]. The term VMAT is used henceforth to describe a rotational irradiation technique in which the gantry speed, dose rate and MLC shape are varied during the optimization.

Recent work [8, 9] has suggested that a hybrid technique which combines multiple gantry angles (greater than 15) and at least one level of intensity modulation (segment) per gantry angle is an optimal solution: the solution space in which the inverse plan optimiser may search is extended [8]. Bratengeier [9] suggested that such a hybrid methodology could be used for older linear accelerators (linacs) which are IMRT-capable, but not VMAT-capable. Thus, the treatment delivery time could be potentially decreased by forming subsequent segments whilst the gantry rotates between adjacent gantry angles analogously to static or “step and shoot” IMRT. It has been proposed to increase the number of gantry angles to achieve an IMAT-like irradiation for older linacs which can only deliver fixed segment (“step and shoot”) IMRT treatments [9]. However, the potential benefits may be outweighed by the data handling time required by the linac and record and verify system [9]. Similarly, recently developed techniques have been described using very high dose rate digital linac, wherein segment shapes are delivered in a quasi-arc manner [10].

A solution has been recently proposed [11, 12] to employ quadratic programming to perform inverse planning. The described scheme uses a priori knowledge of the type of leaf motion pattern during delivery: in particular, leaf pairs sweep 30-50 times across the projected BEV of the target during the course of a full rotation. The leaf motions, rather than individual leaf positions, over a single arc are enforced to lie between the inner and outer radius of the 2D PTV projection (slice-by-slice) under the condition of two constant leaf speeds during the optimisation process. About 30 and 50 static gantry positions are used to model the arc. Quadratic programming is used to ensure that negative dose effects are avoided in their optimisation scheme [12].

### A. 2-Step IMRT/IMAT

Bratengeier [13, 14] introduced a “2-Step IMRT method”, which considers three kinds of segments for IMRT derived from a topological analysis of the planning treatment volume (PTV) and organ-at-risk (OAR): PTV-conformal segments (“zeroth-order segments”, S0), segments irradiating the PTV but entirely blocking the OAR (“first-order segments”, S1), and additional narrow segments adjacent to the OAR to compensate the underdosage (“second-order segments”, S2). This is the simplest approximation of the analytical solution to a constellation of cylindrical OAR surrounded by a cylindrical PTV, sharing a common axis [15]. A description of manual 2-Step generation and subsequent DMPO optimization is described elsewhere [16, 17].

It has been demonstrated that 2-step IMRT and 2-step IMAT plans have the further advantage that their segment forms are more intuitive than those currently created by commercially available optimizers, and that the former techniques lend themselves to inter-fraction adaption [18], or indeed intra-fraction. Moreover, it has been demonstrated [19] that the 2-Step technique can result in fewer segments and monitor units for the same plan quality. The 2-Step IMRT method has been extended with adaptation rules [20] to account for changes in the shape of target volume (TV) and organ-at-risk (OAR) (“2-Step adaptation”): using 3D information from the computed tomography (CT), the widths of second-order segments are adjusted to preserve the total number of monitor units.

An implementation of the 2-step IMAT technique has been recently described [21] by combining the PRISM TPS (University of Washington, Washington, USA) with Matlab (Mathworks, Natick MA, USA), the latter performing the segment weight optimization. The described method is limited to IMAT. Moreover, unlike the current work, they did not constrain the generated segment forms to ensure delivery on the linac. In contrast, the software described in the current work is written in the C++ programming language to determine initial and/or adapted IMRT/IMAT segment forms, and employs a commercial clinical treatment planning system, Pinnacle3<sup>TM</sup> (Philips Medical Systems, Fitchburg, WI, USA), to optimise 2-Step IMAT and IMRT plans. Moreover, the software can be readily extended to be compatible with other treatment planning systems, assuming that those planning systems allow for “seeding” the optimizer with initial segment shapes. To date, this has been attempted by one of the authors with Oncentra MasterPlan v4.3.0 (Elekta AB, Stockholm, Sweden) and Eclipse v10.0 (Varian Medical Systems Palo Alto, CA, USA). Unfortunately the aforementioned treatment planning systems (TPS) do not currently permit the seeding of the optimizer. The scope of this article is limited to the description of the software modules and the subsequent preliminary testing of segment form generation, segment form sequencing, and their further optimization into the TPS: it does not attempt to describe a treatment planning study. Rather this work describes the computational foundation upon which further retrospective treatment planning studies are based [22, 23]. Moreover, [22, 23] describe treatment plan adaption of 2-Step IMRT/IMAT plans on the basis of significant changes to the PTV-OAR constellation determined by cone beam CTs, and compare the resulting adapted plans with a newly optimized plan for the adapted PTV-OAR constellation. The adaptation is only made feasible by the automatic generation of 2-Step segment enabled by the C++ software described in this work.

## II. MATERIALS AND METHODS

A schematic diagram showing data flow between the Pinnacle3<sup>TM</sup> TPS and the in-house C++ software is shown in Fig. 1. The Pinnacle3<sup>TM</sup> (Philips Medical Systems, Fitchburg, WI, USA) TPS v9.1 (non-clinical) and v9.2 (clinical) with the DMPO<sup>TM</sup> optimizer module (RaySearch Laboratories, Stockholm, Sweden) was used. The TPS was installed on a Dual Opteron<sup>TM</sup> server (AMD Inc., Sunnyvale, CA, USA) (2.8 GHz CPU, 16 GB RAM) running the Solaris<sup>TM</sup> 11 operating system (Oracle Corporation, Redwood Shores, CA, USA). The Synergy S<sup>TM</sup> (Elekta AB, Stockholm, Sweden) linear accelerator (linac) and BeamModulator<sup>TM</sup> (Elekta AB, Stockholm, Sweden) MLC have been commissioned in the TPS at the University Hospital Wuerzburg (UKW). The MLC with 40 leaf pairs (4mm), capable of delivering both IMRT and VMAT treatment plans, is henceforth referred to as S4 MLC.

A C++ software was written and tested using the Eclipse CDT development environment (Eclipse Foundation) and the 64-bit gcc compiler (branch 4.4.1) under the 64-bit SuSE Linux 11.2 operating system running on a 64-bit Intel Celsius (Intel Corporation, Santa Clara, CA, USA) PC (4 x 2.66GHz Intel Xeon CPU with 4GB RAM). Dynamic memory allocation and deallocation was performed using the Standard Template Library (STL) vector class, which provides efficient random, constant time, access to large (dynamically resizable) arrays of objects [24]. Generic object classes were declared for POINT, POLYGON, STRUCTURE, LINAC, MLC, BEAM, CONTROL POINT, BEAMLET, and LEAF. Henceforth, C++ data items and classes will be written using capital letters in order to distinguish them from their physical or geometric counterparts.

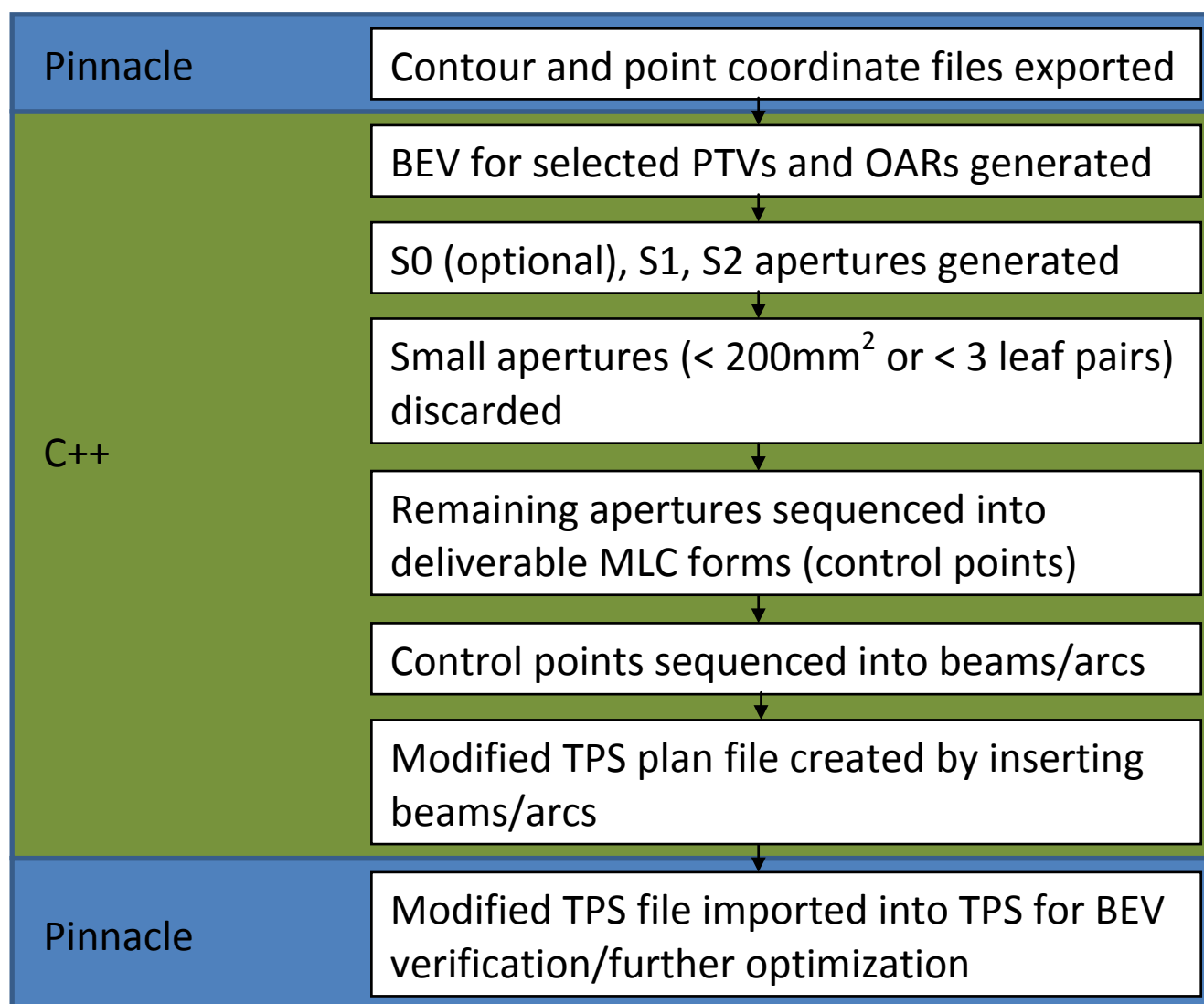


Fig. 1 Schematic diagram showing data flow between the Pinnacle3™ TPS and the in-house C++ software

#### A. Overview of Class Hierarchy

The hierarchical structure of the aforementioned C++ classes will be described in the following paragraphs, grouped according to their types: structural, linac-related and beam-related.

##### 1) Structure, Polygon, and Point

The above classes are grouped together in a hierarchical manner. For instance, the STRUCTURE class comprises an array of POLYGON objects, which in turn comprise an array of POINT objects. Each POINT object comprises the 3D coordinates of a particular point. In this manner, 3D structures, viz. PTV or OAR, are represented as a plurality of closed polygons with at least one polygon corresponding to a particular computer tomography (CT) slice. If a structure is split, for example it bifurcates, then two polygons are defined in the corresponding CT slices. The STRUCTURE class further comprises information regarding the structure name and type (PTV or OAR). This information is provided by the user when employing the software: the PTV(s) and OAR(s) are manually selected from a list of structures found in the TPS structure file.

##### 2) Linac and MLC

The Linac class describes the key parameters of the linac (photon energy, TPS commissioned dose rate(s), VMAT capable, IMRT capable) and also comprises a MLC object. The MLC class comprises the integer number of leaf pairs LP, the maximum field size FS, the maximum permitted leaf overtravel OT, the park position of the leaves PP, in addition to the leaf boundary positions LB. Thus for the S4 MLC one has 40 (LP), 210,160 (FSx, FSy), -105(OT), 110(PP), -80, -76...0, 4...80 (LB0...LBLP-1). Whilst the above classes were developed with the linac and multi-leaf collimator combination available at the UKW in mind, they can be readily tailored to the specific hardware and software available in another hospital. For example, to define a new MLC one simply creates a text file containing the above parameters. Furthermore, generic classes for processing the treatment planning system plan file structure were created.

### 3) Beam, Control Point, Beamlet, and Leaf

Moreover, the BEAM class comprises a number of CONTROL POINTS (monitor units, MU, open segment area, nominal dose rate, NDR, gantry angle, GA, collimator angle, CA, couch angle, COA) which in turn comprise an array of BEAMLETS, open leaf pairs, which comprises a left and a right leaf positions.

### B. PTV/OAR Mask Generation

ROI files (plan.roi), containing coordinate tuples for all manually contoured structures, as well as the points files (plan.Points) which contain the coordinates of all auxiliary points defined for the plan during the course of treatment planning including the isocentre, stored by the TPS were read into the in-house software. The user can select the PTV(s) and OAR(s) from the list of structures found in the aforementioned ROI file. Subsequently, a BEV (perspective) projection for all selected structures and each beam (collimator and gantry angle) required for the plan is determined and stored as a binary mask having the dimensions (in millimetres) of the commissioned MLC, i.e. each binary pixel or bixel represents an area of 1 mm x 1 mm in the projection plane. The bixels take the value “0” outside, or “1” inside the structure.

### C. Aperture Generation

The resulting PTV/OAR masks were subsequently processed by combining simple logical operations “union” ( $\cup$ ) i.e. binary “OR”, “intersection” i.e. binary “AND” ( $\cap$ ), and “not” ( $\neg$ ). In addition, “margin” and “dilation” operators were defined to expand the borders of the respective structure using user specified margins (left, right, superior and inferior) expressed in bixels (mm). In a first step, the corresponding S0, S1 and S2 apertures were generated for each PTV and OAR pair, pq. At this point we are careful to distinguish apertures, the “raw” 2-Step forms derived from logical operation upon the masks, from sequenced deliverable (due to physical limitations such as leaf overtravel) MLC forms. The order S0, S1 and S2 as well as the parent PTV-OAR structures are associated with the aperture for subsequent filtering and identification purposes.

#### 1) Zeroth Order Apertures $S0_{eff-pq}$

The effective S0 aperture mask  $S0_{eff-pq}$  was derived by limiting the expansion of the PTV mask  $M_p$  merely to those regions outside the OAR mask  $M_q$ .

$$S0_{eff-pq} = M_p \cup (\text{margin}_R(M_p) \cap \neg \cup M_q)$$

Thus the zeroth order segment tends to be extended in the superior-inferior direction in regions abutting, but not intersecting  $M_q$  - see Fig. 2(b). The resulting aperture is sequenced into deliverable MLC segments comprising at least 3 leaf pairs and 200mm<sup>2</sup>, see below.

#### 2) First Order Apertures $S1_{eff-pq}$

The first order apertures are derived by blocking out (subtracting) the parent OAR q. The effective S1 aperture mask  $S1_{eff-pq}$  was derived from the respective  $S0_{eff-pq}$  as follows,

$$S1_{eff-pq} = S0_{eff-pq} \cap \neg(\cup M_q)$$

Thus, the resulting aperture tends to comprise two sub-areas, left and right of  $M_q$  see Fig. 2(c) for details.

#### 3) Second Order Aperture $S2_{eff-pq}$

Similarly the S2 aperture mask was derived as follows,

$$S2_{eff-pq} = M_p \cap (\text{dilation}_B(M_q) \cap \neg M_q)$$

In the simplest case, the expansion performed by the dilation operator is constant for all rows within the mask. In other words, the resulting aperture consists of two narrow areas left and right of  $M_q$  - see Fig. 2(d). This appears to be adequate for many tumour localisations, where the topology of the OAR and PTV is simple. However, for breast cases this simple approximation needs to be replaced by a more elaborate scheme  $B(R_{OAR}, R_{PTV})$  which accounts for the radii of the PTV and OAR such that the degree of dilation tapers cranially [13, 14]. The resulting apertures were subsequently sequenced into deliverable MLC segments. A schematic of a simple PTV-OAR constellation is shown in Fig. 2(a), and its resulting 2-Step apertures are shown in Fig. 2(b)-(d).

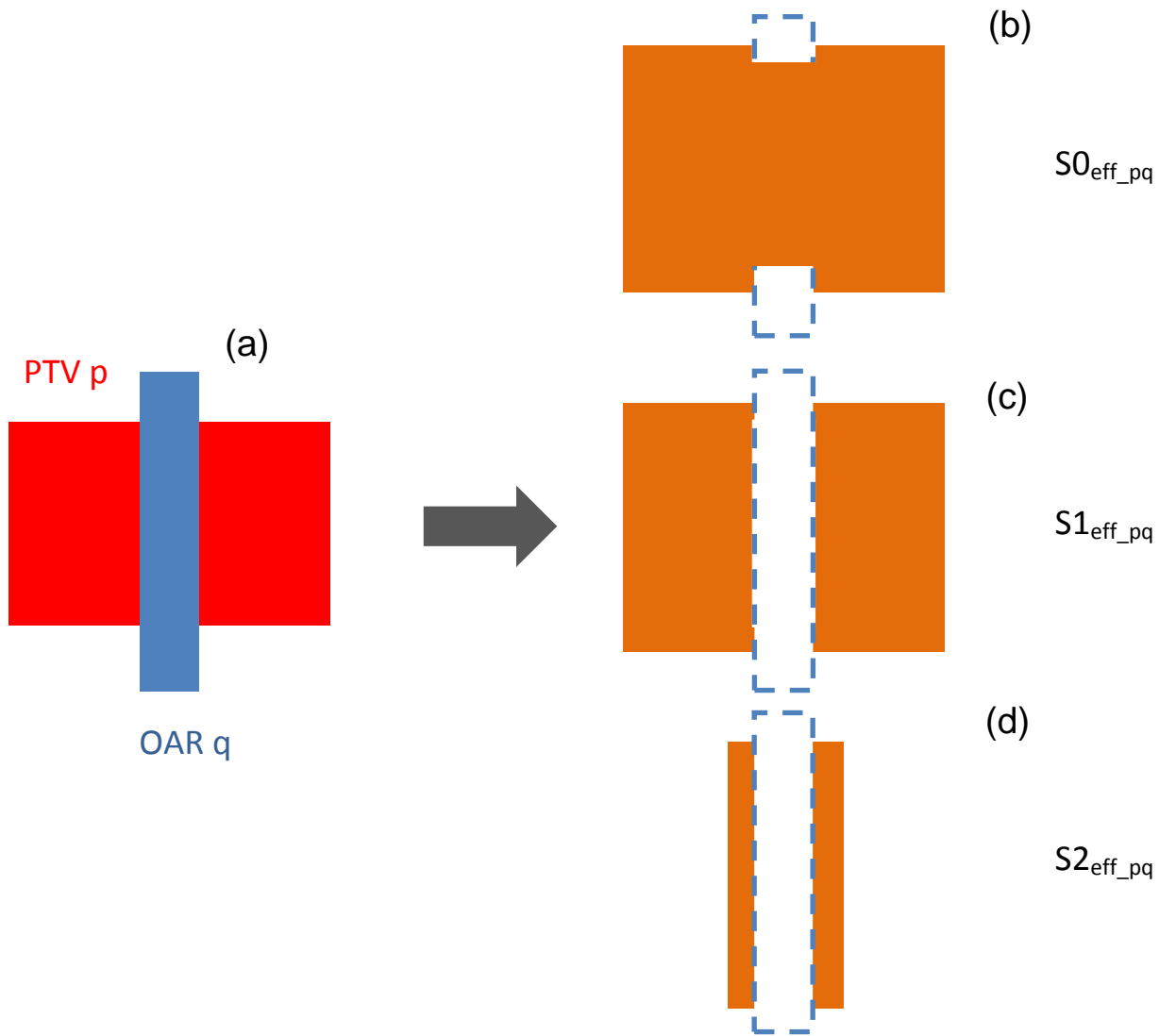


Fig. 2 Schematic diagrams of (a) original PTV-OAR (pq) arrangement, (b) resulting raw 2 step apertures  $S0_{eff\_pq}$  (zeroth order), (c)  $S1_{eff\_pq}$  (first order) and (d)  $S2_{eff\_pq}$  (second order). The typical “H” shape for the zeroth order is shown, and it corresponds to the expanded regions which lie outside OAR q - dashed blue line.  $S1_{eff\_pq}$  shows the typical left-right division relative to OAR q.  $S2_{eff\_pq}$  slender segments which are parallel to projected OAR q

#### D. Sequencing $S0$ , $S1$ and $S2$ Apertures into Deliverable MLC Forms

The generated apertures ( $S0_{eff\_pq}$ ,  $S1_{eff\_pq}$ ,  $S2_{eff\_pq}$ ) for all PTV-OAR pairs were subsequently sequenced into deliverable MLC forms. This procedure is shown schematically in Fig. 3 and in flow diagram in Fig. 4. Each aperture is first scanned top to bottom from left to right, identifying each opening (beamlet) for that row: each row may contain a few beamlets (step 1 in Fig. 4). A beamlet opening is found by a Heaviside transition (0 to 1) in adjacent columns to identify the left edge,  $LL$ , of the beamlet and similarly by a Heaviside transition (1 to 0) for the right edge,  $LR$ . Furthermore, the first and last two columns are additionally checked to ensure that no opening at either the  $LL$  or  $LR$  of the leaf banks is omitted, viz. “1 1” is assigned to the respective columns. After all beamlets for each row have been identified, the beamlets are subsequently assigned to a MLC segment. Starting with the first beamlet found in row  $j$ , the first row (Fig. 4 step 2) for which a beamlet has been identified, this beamlet ( $b_{0,j}$ ) is always assigned to the first MLC segment ( $MLC_0$ ) (Fig. 4 step 3). If  $is-1$  additional beamlets are found in the same row  $j$ , they are automatically assigned to the second ( $MLC_1$ ) or subsequent MLC ( $MLC_k$  where  $0 < k < is$ ) segment for the current aperture (Fig. 4 step 3). All beamlets identified in subsequent rows ( $j+1$  to  $LP-1$ ) are tested to determine whether they belong to one of the existing MLC ( $MLC_{is-1}$ ) segments.

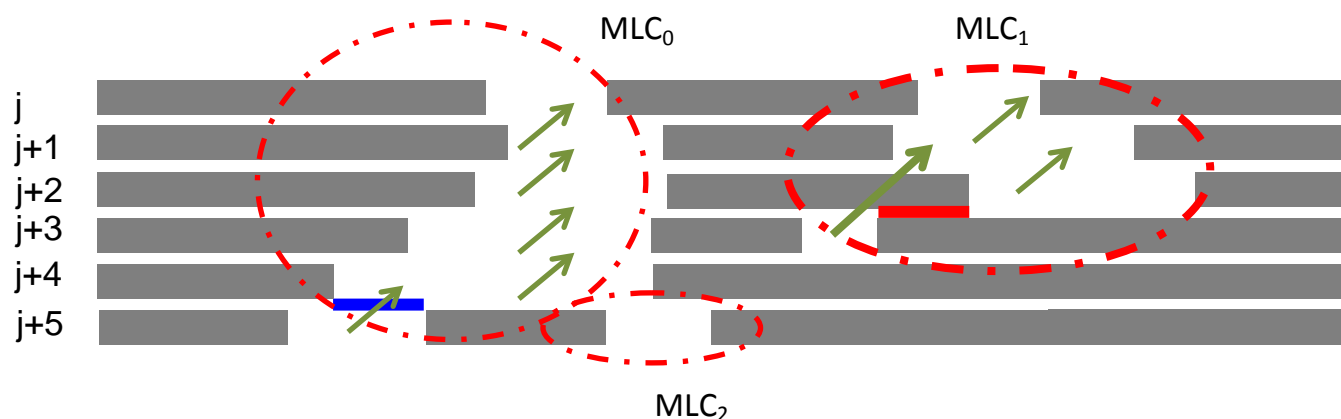
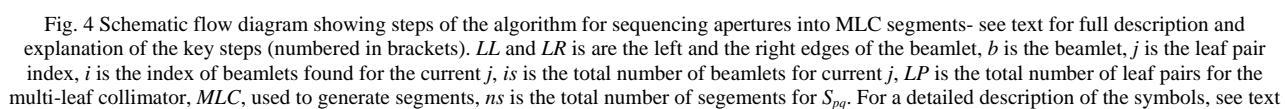


Fig. 3 Schematic diagram showing the sequencing of a hypothetical 2 step aperture into 3 deliverable MLC segments:  $MLC_0$ ,  $MLC_1$ ,  $MLC_2$  (red dashed-dot ellipses). Each row 2-step aperture is scanned top to bottom, left to right to locate beamlets (openings, shown here in white). More than one beamlet may be present in a row (rows  $j$  to  $j+3$  and  $j+5$ ). In row  $j+1$  the two openings are assigned to  $MLC_0$  and  $MLC_1$  respectively (green arrow). In row  $j+5$  two beamlets are found which potentially belong to  $MLC_0$ . In this instance the number of overlapping bixels between the opening in row  $j+4$  and the openings in row  $j+5$  is determined: the opening with the greatest overlap (blue) is selected. A third MLC form,  $MLC_2$ , is created for the remaining opening in row  $j+5$ . In row  $j+3$ , the opening with negative overlap (red) is assigned to  $MLC_1$ . The identified MLC forms  $MLC_0$ ,  $MLC_1$ , and  $MLC_2$  are subsequently filtered and sequenced—see text for details

The beamlets in the rows  $j+1$  to  $LP-1$  are assigned to segments based on the overlap with existing segments. If the beamlet and the segment have common open (binary true) bixels, the overlap is the number of these bixels (Fig. 4 step 6). Otherwise, the overlap is the negative distance in bixels from the beamlet to the segment (Fig. 3). For each existing segment  $MLC_k$ , the beamlet with maximum overlap (which can also be negative) among the beamlets in the row  $j$  is found and assigned to  $MLC_k$ , and for the next segment  $MLC_{k+1}$  the candidate among the remaining beamlets is searched (Fig. 4 step 4). If the beamlet cannot be assigned to any existing segment, a new segment  $MLC_{ns+1}$  is generated (Fig. 4 step 5) and added to the collection of segments. For masks with disconnected parts, this approach generates segments which have corresponding disconnected parts. If the MLC cannot deliver such segments, for example opposing adjacent leaves are not allowed to overlap, the disconnected parts are connected by opening the leaves. This approach has the advantage of generating fewer segments, which improves the dosimetric quality of the plan.

Typically, two  $S1$  sequenced MLC segments will be produced per PTV-OAR pair: one  $S1$  segment to the left and one to the right of the parent OAR  $q$ , as depicted schematically  $S1_{eff,pq}$  in Fig. 2(c). As additional information, the chirality of the sequenced  $S1$  and  $S2$  segments (left or right) is determined relative to their parent OAR  $q$ . This merely involves determining whether  $LL$  and  $LR$  of the segment lie to the left or right of  $LL$  and  $LR$  for mask  $M_q$ . This information is required for generating IMAT-like control point sequences in which only left, or right, segment types are selected (see next section). Finally the open area of  $MLC_k$  is determined by summing the individual beamlet areas (opening width ( $LR-LL$ ) x leaf height). If the calculated open area is smaller than  $200 \text{ mm}^2$ , or the number of open leaf pairs is less than 2,  $MLC_k$  is deemed invalid and it is discarded. This is done primarily for dosimetric accuracy, since small radiation fields are difficult to measure as part of a quality assurance program using current generation of 2D measurement arrays due to their finite spatial resolution: a small spatial shift can have a dramatic effect on the dose distribution. Furthermore, it is more efficient to employ a modest number of larger irradiation fields than employing a large number of smaller fields.



### E. Generating Control Point Sequences

The remaining (valid) MLCs are grouped together in control point sequences for each fixed gantry angle (IMRT) or each arc (IMAT). In the case of IMAT, it is not necessary to irradiate all segments of type  $S1$  or  $S2$  for all gantry angles  $\alpha$  [9], since there are equivalent segment forms incident from the opposing gantry angle ( $180^\circ - \alpha$ ). Consequently, it is only necessary to irradiate the left  $l$ , or right  $r$ ,  $S1$  and  $S2$  segments relative to each OAR. Thus, taking the simple example of a single PTV-OAR pair, the following segment sequence could result:

$$\{S0S1_{l/r}S2_{l/r}\}^m,$$

where  $m$  denotes that the enclosed segment sequence is repeated  $m$  times. The  $S0$  segments may be omitted from the sequence for maximal sparing of the OAR, although the dose homogeneity may be consequently degraded. Thus, the control point sequence would be:

$$\{S1_{l/r}S2_{l/r}\}^m.$$

In this way the leaf motion appears to oscillate between the  $S1$  and  $S2$  segment forms along the arc length. A similar leaf motion oscillation is observed in [11, 12], resulting from limiting the leaf motion between inner and outer PTV radius over a single arc employing the optimisation scheme described therein.

### F. Exporting Generated Segment Sequences to the TPS

In order to generate a 2-Step plan, an existing Pinnacle plan file (plan.Trial) is read by the software. If more than one plan variant, or trial, exists in the plan file, the user is prompted to select a trial which is to be modified. The plan.Trial files are ASCII files with structure resembling the tag structure of the DICOM format. In the case of IMRT, every trial contains a number of beams, each corresponding to a fixed gantry angle, where each beam has a number of control points describing the segment shape and number of monitor units (MU) to be delivered per segment. Conversely, for VMAT there is at least one beam, or arc, containing one control point for each gantry angle used in optimising the planned arc. The number of control points per arc varies, typically between 59-179, depending on the total angle of the particular arc and the angular spacing between control points selected in the optimisation. Thus, the 2-Step plan replaces existing control points (MLC segment forms) with those generated by the in-house software as described above. It should be emphasised that this plan file contains only the gantry beam angles and segment forms: it is in no way an optimised clinical plan for patient treatment. This additional optimisation step would need to be performed to generate a clinically acceptable plan. In order to fully test the C++ software this step was performed merely to verify that the generated treatment plan is considered valid by the TPS, i.e. it can be further optimized by the TPS, and not to generate clinically acceptable patient plans. This is subject of other work by the authors [22, 23].



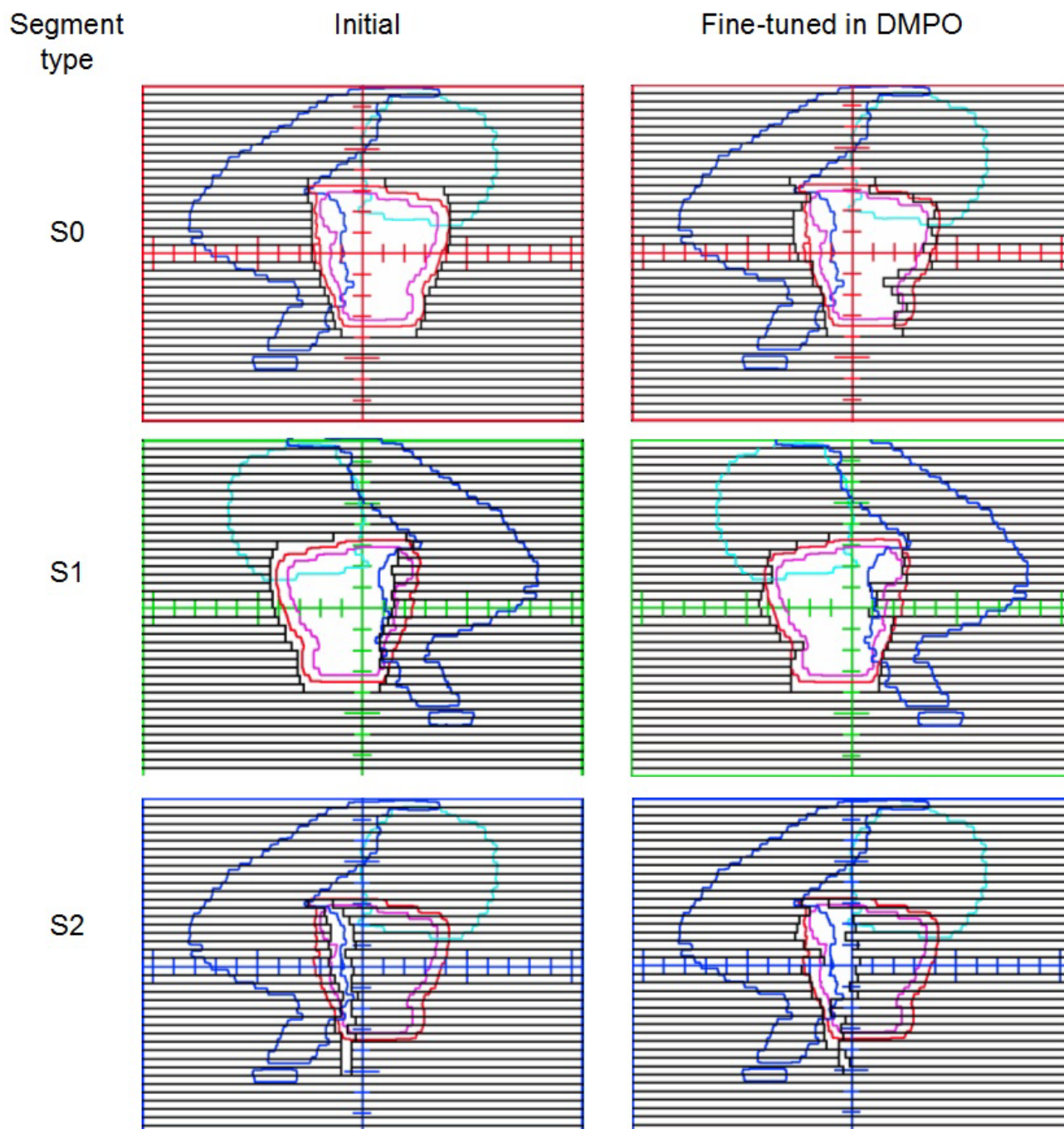


Fig. 5 Pinnacle<sup>3</sup> BEV, showing C++ generated 2-step segments (left column) and corresponding fine tuned DMPO optimized 2-Step segments (right column) for an example prostate case: upper row  $S_0$  zeroth order; middle row  $S_1$  second order and bottom row  $S_2$  second order right. PTV is depicted in red, GTV in pink, rectum in dark blue and bladder in cyan. The origin of the axes shows the position of the isocentre. The tick marks are in cm

In the future, a separate module will independently verify the degree of congruence of the generated segment shapes with their parent PTV-OAR pairs, resulting in a visual traffic-light-like warning for the planner: red, amber or green to signify to what degree the segment shapes are acceptable. This functionality will be required when 2-Step IMRT/IMAT plans are adapted to the daily patient geometry, to provide the medical physics expert (MPE) or radiation oncologist with a succinct overview of the adapted plan. For the purposes of initial testing, the  $S_0$ ,  $S_1$ ,  $S_2$  aperture masks were visually inspected, by writing the data as .png image files, and the resulting filtered and sequenced segment forms were viewed within the TPS in order to ensure that the resulting plan file could be imported.

### G. Clinical Test Cases

Six prostate cases with simultaneous integrated boost (SIB) concept [25] comprising PTV and Boost target volumes were employed for preliminary testing of the software with a simple PTV-OAR constellation from clinical data. Each plan consisted of seven beams at equally distributed gantry angles in accordance with the standard operating procedures for planning at UKW. Furthermore, two more challenging vertebral body cases were also employed. These cases also consisted of a SIB for paraspinal metastases abutting the spinal cord. These cases were to be planned with nine beams at equally distributed gantry angles per the standard operating procedures at UKW. It is expected that for such a PTV-OAR constellation, where very steep dose gradients are essential, that the potential benefit of 2-Step IMAT/IMRT will be seen. However, this working hypothesis will need to be tested in a comprehensive planning study.

The computation time taken to generate the segments was recorded. In addition, the segment shape was visually checked using the TPS, to ensure that the algorithm performed in accordance with its design specification. This step will be automated in the future, by an independent software program.

## III. RESULTS

The preliminary results for the segment generation are presented below.

### A. Segment Generation Time

#### 1) Prostate

The average time taken per generated segment was  $36 \pm 6$ ms, employing the current hardware described supra, for seven beam directions for both PTV and Boost (nominally total of 70 segments:  $S0$ ,  $S1$ ,  $S2$ ), see also Table 1. This time includes the time taken to filter all generated segments according to the aforementioned criteria for valid segments, see the Materials and Methods section. The initial masks,  $S0$ ,  $S1$ , and  $S2$  were inspected and their resulting segment forms were viewed in the TPS and found to be correctly generated.

Fig. 5 shows an example with the gantry positioned at the side ( $GA=90^\circ$ ). To verify that the generated 2-Step plan imported into the TPS was valid, a single optimization was performed: if the segments were invalid the optimization could not be performed. The authors stress that the aim of this additional step is not to generate a clinically acceptable patient plan.

The left column of Fig. 5 shows the raw 2-Step ( $S0$ ,  $S1$ ,  $S2$ ) segments as imported into the TPS. The right column shows the resulting DMPO optimized 2-Step segments, after 50 DMPO iterations, of the respective order. One can see that the initial form of the zeroth order is largely untouched: the right hand leaves being shifted medially. The first order segment retains their general shape: four leaves near the centre right of the field are shifted medially. The second order segments,  $S2$ , are more significantly altered, however, retaining their second order characteristics. The DMPO algorithm appears to correct the subtle 3D relationships between PTV and OAR, and to smooth out the dose plateau. However, a detailed analysis is beyond the scope of this paper.

TABLE 1 SUMMARY OF SEGMENT GENERATION TIME FOR PROSTATE CASES 1-6

Case	Time [s]	Segments
1	1.9	70
2	2.3	70
3	3.3	70
4	2.5	70
5	2.5	70
6	2.5	70

#### 2) Paraspinal Metastases

For these cases, three arcs were generated with  $2^\circ$  spacing per control point (179 segments for a complete rotation). The total time taken was 13.1 and 12.0 seconds ( $S0$ ,  $S1$ ,  $S2$ : 537 segments) or 24ms and 22ms per segment respectively.

## IV. DISCUSSION

The first phase of the computerization of 2-Step planning, automatic segment generation, is now complete. This work demonstrates that the algorithm accurately generates segment shapes for both “step and shoot” IMRT and VMAT expeditiously, greatly improving the efficiency in performing 2-Step based planning studies since segments must no longer be manually defined. Thus, on the basis of current hardware, segments can be generated within 10 seconds for a typical seven-field IMRT beam configuration for plans comprising two target volumes and a single dominant OAR. In the case of 2-Step IMAT, approximately 13 seconds is required to generate three complete arcs, each comprising 179 segments of  $S0$ ,  $S1$ , and  $S2$ . Furthermore, since the physical limitations of the MLC are taken into account, the plans generated can be irradiated by the

Synergy linear accelerator [22]. Moreover, implementation is potentially extendible to other TPS, linear accelerators and MLCs, although further work needs to be done to determine whether it is possible to “seed” the TPS optimiser with 2-Step segments for further optimisation. This enables a comprehensive treatment planning comparison of the 2-Step IMRT/IMAT and IMRT/VMAT plans generated in commercial software [22, 23]. One further aspect to be investigated is collimator angle optimisation in order to minimise the total number of segments generated and MUs required to deliver the prescribed dose.

The second phase, computer-implemented plan adaption, is currently work in progress and will be the subject of another publication [22, 23]. In particular, the merits of monitor-unit-preserving versus monitor unit varying adaption will be more comprehensively explored. Moreover, before the software is rolled out into the clinic, a suite of tools needs to be developed to assist the medical physics expert (MPE) and radiation oncologist to assess the quality of adapted plans and to alert the MPE if preset action levels are exceeded.

## V. CONCLUSION

A suite of C++ programs has been developed to process Pinnacle3<sup>TM</sup> TPS structure files, perform the geometric analysis and sequence the resulting 2-Step shapes for import into the TPS. This procedure requires less than ten seconds for IMRT,  $2.5 \pm 0.5$ s for 7-Field SIB prostate cases ( $36 \pm 6$ ms per segment), and about 13 seconds for 3-arc single PTV-OAR pair IMAT (24ms and 22ms per segment) using the current hardware and software. Thus, with the software tool described in this work 2-Step based treatment planning can now be routinely used for retrospective treatment planning studies. This enables 2-Step-based radiotherapy planning to move towards clinical routine. The support of DICOM RT format is planned to be added in the next iteration of the project.

## ACKNOWLEDGMENTS

This work was in part supported by the German Research Foundation (Deutsche Forschungsgemeinschaft—DFG Project code DFG BR 3460/2-1BR) and the Wilhelm Sander Stiftung (Project Code 2010.102.01). The authors thank the Philips Corporation for making available research stations with Pinnacle3<sup>TM</sup> version 9.1.

## REFERENCES

- [1] K. Otto, “Volumetric modulated arc therapy: IMRT in a single gantry arc”, *Med Phys*, vol. 35, pp. 310-317, 2008.
- [2] C. X. Yu, “Intensity-modulated arc therapy with dynamic multileaf collimation: an alternative to tomotherapy”, *Phys Med Biol*, vol. 40, pp. 1435-1449, 1995.
- [3] T. Bortfeld and S. Webb, “Single-Arc IMRT?”, *Phys Med Biol*, vol. 54, pp. N9-N20, 2009.
- [4] K. Bzdusek, H. Friberger, K. Eriksson, B. Hardemark, D. Robinson and M. Kaus, “Development and evaluation of an efficient approach to volumetric arc therapy planning”, *Med Phys*, vol. 36, pp. 2328-2339, 2009.
- [5] M. Guckenberger, A. Richter, T. Krieger, J. Wilbert, K. Baier and M. Flentje, “Is a single arc sufficient in volumetric-modulated arc therapy VMAT for complex-shaped target volumes?”, *Radiother Oncol*, vol. 93, pp. 259-265, 2009.
- [6] W. F. Verbakel, S. Senan, F. J. Lagerwaard, J. P. Cuijpers and B. J. Slotman, “Comments on ‘Single-Arc IMRT?’”, *Phys. Med. Biol*, vol. 54, pp. L31-L34, 2009.
- [7] A. Bertelsen, C. R. Hansen, J. Johansen, and C. Brink, “Single arc volumetric modulated arc therapy of head and neck cancer”, *Radiother Oncol*, vol. 95, pp. 142-148, 2010.
- [8] R. Li and L. Xing, “Bridging the gap between IMRT and VMAT: Dense angularly sampled, and sparse intensity modulated radiation therapy”, *Med Phys*, vol. 38, pp. 4912-4919, 2011.
- [9] K. Bratengeier, M. Gainey and M. Flentje, “Fast IMRT by increasing the beam number and reducing the number of segments”, *Radiation Oncol*, vol. 6, pp. 170-180, 2011.
- [10] B. J. Salter, V. Sarkar, B. Wang, H. Shukla, M. Szegedi and P. Rassiah-Szegedi, “Rotational IMRT delivery using a digital linear accelerator in very high dose rate ‘burst mode’”, *Phys Med Biol*, vol. 56, pp. 1931-1946, 2011.
- [11] W. Hoeghele, R. Loeschel and P. Zygmanski, “An alternative VMAT with prior knowledge about the type of leaf motion utilizing projection method for concave targets”, *Med Phys*, vol. 36, pp. 3764-3774, 2009.
- [12] W. Hoeghele, R. Loeschel, N. Merkle and P. Zygmanski, “An efficient inverse radiotherapy planning method for VMAT using quadratic programming optimization,” *Med Phys*, vol. 39, pp. 444-454, 2012.

- [13] K. Bratengeier, "2-Step IMAT and 2-Step IMRT: A geometrical approach", *Med Phys*, vol. 32, pp. 777-785, 2005.
- [14] K. Bratengeier, "2-Step IMAT and 2-Step IMRT in three dimensions", *Med Phys*, vol. 32, pp. 3849-3861, 2005.
- [15] A. Brahme, J. E. Roos and I. Lax, "Solution of an integral equation encountered in rotation therapy", *Phys Med Biol*, vol. 27, pp. 1221-1229, 1982.
- [16] K. Bratengeier, J. Meyer and M. Flentje, "Pre-segmented 2-Step IMRT with subsequent direct machine parameter optimisation – a planning study", *Radiation Oncol*, vol. 3, pp. 38-44, 2008.
- [17] K. Bratengeier, J. Meyer, F. Schwab, D. Vordermark and M. Flentje, "Steep dose gradients for simultaneous integrated boost IMRT", *Zeitschrift für Medizinische Physik*, vol. 19, pp. 129-35, 2009.
- [18] K. Bratengeier, B. Polat, M. Gainey, P. Grewenig, J. Meyer and M. Flentje, "s ad-hoc plan adaptation based on 2-Step IMRT feasible?", *Radiother Oncol*, vol. 93, pp. 266-72, 2009.
- [19] M. Gainey, K. Bratengeier and M. Flentje, "Application of 2-Step IMRT to Spinal Tumors: A Preliminary Retrospective Planning Study Comparison with Classical IMRT", World Congress on Medical Physics and Biomedical Engineering, IFMBE Proceedings, Eds Doessel, O, Schlegel, W C 1, pp. 981-984, 2009.
- [20] K. Bratengeier, B. Polat, M. Gainey, P. Grewenig, J. Meyer, and M. Flentje, "Is ad-hoc plan adaptation based on 2-Step IMRT feasible?", *Radiotherapy and Oncology*, vol. 93, no. 2, pp. 266-272 2009.
- [21] J. Sun, T. Y. Chew and J. Meyer, "Two-step intensity modulated arc therapy (2-step IMAT) with segment weight and width optimization", *Radiat Oncol*, vol. 6, pp. 57-66, 2011.
- [22] K. Holubyev, K. Bratengeier, M. Gainey, B. Polat and M. Flentje, "Towards automated on-line adaptation of 2-Step IMRT plans: QUASIMODO phantom and prostate cancer cases", *Radiat Oncol*, vol. 8, pp. 263-275, 2013.
- [23] K. Holyubev, M. Gainey, K. Bratengeier, B. Polat and M. Flentje, "Generation of prostate IMAT plans adaptable to the inter-fractional changes of patient geometry", in press *Physics in Medicine and Biology*.
- [24] H. Schildt, *C++: The Complete Reference*, Fourth Edition, New York: McGraw-Hill/Osborne, pp. 834-836, 2003.
- [25] M. Guckenberger and M. Flentje, "Intensity-modulated radiotherapy (IMRT) of localized prostate cancer: a review and future perspectives", *Strahlenther Onkol*, vol. 183, pp. 57-62, 2007.